Pergamon

Int. J. Heat Mass Transfer. Vol. 41, No. 11, pp. 1559–1572, 1998

Printed in Great Britain
0017–9310/98 $19.00+0.00

PII: S0017–9310(97)00224–X

Transition to oscillatory natural convection of cold water in a vertical annulus

C. J. HO† and F. J. TU

Department of Mechanical Engineering, National Cheng Kung University, Tainan, Taiwan 701, Republic of China

(*Received* 13 *January* 1997 *and in final form* 1 *July* 1997)

Abstract—In the present study laminar transition to oscillatory convection of cold water in a vertical annulus of aspect ratio 8 and radius ratio 2 is investigated by direct numerical simulations for two values of density inversion parameter, $\theta_m = 0.4$ and 0.5. The vertical walls of the annulus are maintained at constant but different temperatures, while the horizontal walls are assumed adiabatic. Numerical results manifest that the buoyancy-driven flow in the annulus experiences a Hopf bifurcation into a periodic oscillation regime at the critical Rayleigh numbers, which are dependent on the density inversion parameter. The critical Rayleigh number for $\theta_m = 0.4$ is found to be more than two times of that corresponding to $\theta_m = 0.5$. Nature of the transition has also been identified by examining the contributions made by the flow shear and/or the buoyancy force to the generation of fluctuating kinetic energy for the self-sustained oscillatory convection in the annulus.

INTRODUCTION

This article presents a numerical study concerning laminar transition from steady state into oscillatory natural convection of water near its density maximum (cold water) in a tall differentially heated cylindrical annulus of aspect ratio 8, as illustrated schematically in Fig. 1. The density of cold water is known to feature, unlike the ordinary fluids, a nonlinear density-temperature relationship, having their maximum density at a temperature T_m above the melting temperature. At sea-level atmospheric pressure T_m is about 4°C. Under influence of the density inversion phenomenon of cold water (near 4°C), peculiar behaviors, such as multicellular flow structure and heat transfer extreme, of the buoyancy-driven convection flow and heat transfer in enclosure have been found. Due to the important role it played in many technical and engineering applications, natural convection problems of cold water in vertical rectangular and horizontal cylindrical annular enclosures have received considerable research attentions. Fairly thorough reviews of the works concerning these two configurations can be found in previous studies [1–5].

Relatively little attention has been given to natural convection of cold water in vertical annulus formed by two co-axial vertical cylinders. Lin and Nansteel [6] presented a numerical study of steady natural convection in cold water-filled vertical annuli of various aspect ratios in the range 1–8. It was found that both the density inversion phenomenon and the annulus curvature can strongly affect the buoyancy-driven flow structure and heat transfer in the annulus. Ho and Lin [7] carried out an extensive numerical work on cold water-filled vertical annuli subjected to a mixed boundary condition of constant heat flux on the inner wall. The aspect ratios of the annulus considered are in the range between 0.5 and 8 with the radius ratio varying between 1.2 and 10. The mixed boundary conditions were found to have a strong effect on the geometric dependence of the heat transfer characteristics and flow structures of cold water inside the annulus. In a tall annulus of aspect ratio 8, a multicellular flow behavior of cold water was found to arise at the Rayleigh number of 10^5 with a wavy maximum density contour. It can be further noticed that the foregoing studies were focused on the steady-state natural convection of cold water in vertical annulus. No efforts apparently exist which consider the

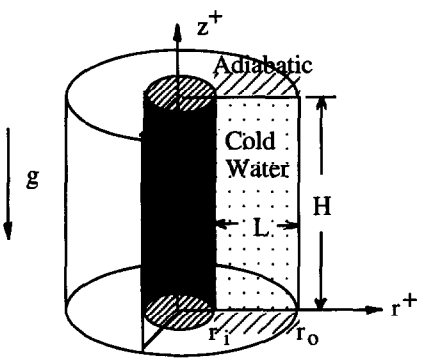

Fig. 1. Schematic diagram of physical configuration and coordinate system of natural convection of cold water in a vertical annulus of aspect ratio 8.

†Author to whom the correspondence should be addressed.

NOMENCLATURE

A	aspect ratio H/L
b	exponent in the density equation
f^+	frequency
f	dimensionless frequency, f^+L^2/α
g	gravitational acceleration
H	annulus height
k	thermal conductivity
L	gap width (r_o-r_i)
Nu	Nusselt number
p^+	period, $1/f^+$
p	dimensionless period, $1/f$
P^+	pressure
P	dimensionless pressure, $P^+/[\rho_m(\alpha/L)^2]$
Pr	Prandtl number, ν/α
r^+	radial coordinate
r	dimensionless radial coordinate, r^+/L
Ra_H	Rayleigh number based on annulus height, $g\cdot rsp(\Delta T)^bH^3/(\nu\alpha)$
Ra_L	Rayleigh number based on gap width, $g\cdot rsp(\Delta T)^bL^3/(\nu\alpha)$
r_i	radius of inner wall
r_o	radius of outer wall
RR	radius ratio, r_o/r_i
rsp	coefficient in density equation
t	time
T	temperature
ΔT	temperature difference between inner and outer wall (T_i-T_o)
u_i	velocity component $(i=1,2)$
x_i	coordinate direction $(i=1,2)$
z^+	axial coordinate
z	dimensionless coordinate, z^+/L.

Greek symbols

α	thermal diffusivity
$\delta_{i,j}$	Kronecker delta
θ	dimensionless temperature $(T-T_o)/\Delta T$
θ_m	density inversion parameter $(T_m-T_o)/\Delta T$
ν	kinematic viscosity
ρ	density
τ	dimensionless time, $\alpha t/L^2$
ψ^+	stream function
ψ	dimensionless stream function, $\psi^+/(\alpha L)$
ω^+	vorticity
ω	dimensionless vorticity, ω^+L^2/α.

Superscripts

$'$	fluctuating components
$-$	time-averaged quantity.

Subscripts

cr	critical state
i	inner wall of annulus
m	maximum density or periodically mean value
o	outer wall of annulus.

laminar flow transition into unsteady buoyancy-driven flow of cold water in a vertical annulus. The objective of present study is, therefore, to gain insight into the onset of unsteadiness, under influence of the density inversion of cold water, in a vertical annulus of aspect ratio 8. To this end, direct numerical simulations via a finite difference method have been undertaken to obtain the long-time behavior of the natural convection of cold water in the tall vertical annulus.

MATHEMATICAL FORMULATION

Consider a vertical cylindrical annulus schematically illustrated in Fig. 1, filled with cold water. The height and gap width of the annulus are denoted by H and L, respectively. The inner and outer vertical walls of the annulus are differentially heated at constant uniform temperatures T_i and T_o $(<T_i)$, respectively. The horizontal end walls of the annulus are assumed adiabatic. The cold water in the annulus is considered to be an incompressible, Newtonian fluid for which the Boussinesq approximation is assumed to be valid. Viscous dissipation is neglected. Furthermore, we consider a vertical annulus of sufficiently small values of the radius ratio so that, following the results of linear stability analysis by McFadden *et al.* [8], the buoyancy-driven flow is likely to be axisymmetric. In terms of vorticity, stream function, and temperature, the dimensionless differential equations governing the time-dependent axisymmetric buoyancy-driven flow of cold water in the vertical annulus may be written as

$$\frac{\partial\omega}{\partial\tau}-\frac{\partial}{\partial r}\left(\frac{\omega}{r}\frac{\partial\psi}{\partial z}\right)+\frac{\partial}{\partial z}\left(\frac{\omega}{r}\frac{\partial\psi}{\partial r}\right)$$

$$=Pr\left(\frac{\partial^2\omega}{\partial r^2}+\frac{1}{r}\frac{\partial\omega}{\partial r}-\frac{\omega^2}{r}+\frac{\partial^2\omega}{\partial z^2}\right)-Pr\,Ra_L\frac{\partial\theta^*}{\partial r} \quad (1)$$

$$\frac{\partial^2\psi}{\partial r^2}-\frac{1}{r}\frac{\partial\psi}{\partial r}+\frac{\partial^2\psi}{\partial z^2}=-r\omega \quad (2)$$

$$\frac{\partial\theta}{\partial\tau}-\frac{\partial}{\partial r}\left(\frac{\theta}{r}\frac{\partial\psi}{\partial z}\right)+\frac{\partial}{\partial z}\left(\frac{\theta}{r}\frac{\partial\psi}{\partial r}\right)=\frac{\partial^2\theta}{\partial r^2}+\frac{1}{r}\frac{\partial\theta}{\partial r}+\frac{\partial^2\theta}{\partial z^2} \quad (3)$$

where $\theta^*=|\theta-\theta_m|^b$. In eqn (1) the nonlinear density-

temperature relation of cold water is modeled incorporating a correlation proposed by Gebhart and Mollendorf [9], which is of the form

$$\rho(T) = \rho_m(1 - rsp|T - T_m|^b) \tag{4}$$

where $\rho_m = 999.9720$ kg/m^3, $rsp = 9.297173 \times 10^{-6}$ (°C)$^{-b}$, $T_m = 4.029325$°C, $b = 1.894816$.

The boundary conditions of the present problem are

$$\frac{\partial\psi}{\partial r} = \frac{\partial\psi}{\partial z} = \psi = 0, \quad \text{on all boundaries}$$

$$\theta = 1, \quad r = \frac{1}{RR-1},$$

$$\theta = 0, \quad r = \frac{RR}{RR-1},$$

$$\frac{\partial\theta}{\partial z} = 0, \quad z = 0 \quad \text{or} \quad A. \tag{5}$$

As revealed from the above formulation, for the present problem with the aspect ratio A and the radius ratio RR of the annulus fixed at 8 and 2, respectively, and the Prandtl number $Pr = 12.5$ for cold water the dimensionless parameters include a Rayleigh number Ra_L and a density inversion parameter θ_m. The reason that we chose to perform the simulations in an annulus of aspect ratio of 8 was primarily due to the findings of the earlier study [7], in which a multicellular flow structure of cold water with a wavy maximum density contour arose in this particular aspect ratio.

The heat transfer rates at the thermally active walls of the annulus are presented by the local Nusselt numbers defined as

$$Nu_i = -\left.\frac{\partial\theta}{\partial r}\right|_{r=1/(RR-1)} \tag{6a}$$

and

$$Nu_o = -\left.\frac{\partial\theta}{\partial r}\right|_{r=RR/(RR-1)}. \tag{6b}$$

Moreover, to gain further insight into the mechanism of instability, the governing equation describing the conservation of fluctuating kinetic energy, $(u_i'u_i'/2)$, of oscillatory convection in the annulus [10] can be derived as the following form:

$$\frac{\partial}{\partial\tau}\left(\frac{u_i'u_i'}{2}\right) = \underbrace{-\frac{\partial}{\partial x_j}\left(u_i'\bar{u}_j\bar{u}_i + \bar{u}_j u_i'u_j'/2 + u_j'P + Pru_i'\frac{\partial\bar{u}_i}{\partial x_j}\right)}_{\text{I}}$$

$$\underbrace{+\bar{u}_i\bar{u}_j\frac{\partial\bar{u}_i}{\partial x_j} - Pr\frac{\partial\bar{u}_i}{\partial x_j}\frac{\partial u_i'}{\partial x_j} + Pr\,Ra_L u_i'(\bar{\theta}-\theta_m)^2\delta_{i2}}_{\text{II}}$$

$$\underbrace{-u_i'u_j'\frac{\partial\bar{u}_i}{\partial x_j} + Pr\,Ra_L[2(\bar{\theta}-\theta_m)\theta' + (\theta')^2]\delta_{i2} - Pr\frac{\partial u_i'}{\partial x_j}\frac{\partial u_i'}{\partial x_j}}_{\text{III}} \tag{7}$$

Here, the first and second groups of terms, designated respectively by I and II, on the right-hand side of eqn (7) become vanished, respectively, by integration over the enclosure and integration over one period of oscillation. Only the third group of terms designated by III can contribute to temporal variation of the fluctuating kinetic energy. Specifically, the terms of $-u_i'u_j'\partial\bar{u}_i/\partial x_j$ and $Pr\,Ra_L[2(\bar{\theta}-\theta_m)\theta' + (\theta')^2]\delta_{i2}$ represent the local production of fluctuating kinetic energy due to the mean flow shear and buoyancy forces, respectively; while the term $-Pr\,\partial u_i'/\partial x_j\,\partial u_i'/\partial x_j$ represents the viscous dissipation of fluctuating kinetic energy. It should be noted that for mathematical simplicity a parabolic form of density-temperature relation suggested by Simmons [11] was used in deriving eqn (7) instead of using eqn (4) directly.

NUMERICAL METHOD

The governing differential equations, eqns (1)–(3), were discretized spatially with a finite difference method involving second-order central difference scheme for the diffusion terms while QUICK-2D scheme [12] for the convective terms. A non-uniform mesh, which provides progressively finer grids toward the vertical walls of the annulus, was constructed along the radial direction to accurately resolve gradients in the boundary layers developed along the vertical walls. A uniform mesh was, on the other hand, deployed in the z-direction. Boundary vorticity was treated using Thom formula [13]. The integration of the equations in time was then performed fully explicitly with a second-order accuracy. At each time step, the discretized stream function equations were iteratively solved by a line successive relaxation method until a relative convergence criterion of less than 5×10^{-8} was met. The solution was considered to be converged to steady state if the relative convergence criteria of 10^{-7} and 10^{-8} were, respectively, satisfied for solutions of vorticity and temperature.

Numerical simulations, starting with a predicted steady flow, were performed by increasing gradually the Rayleigh number until an oscillatory behavior was detected. Increases in the Rayleigh number were made in relatively small steps, so that the convective evolution could be followed in detail. The initial conditions for subsequent simulations were those associated with the preceding lower Rayleigh number. Furthermore, to investigate the possibility of hysteresis effects in the transitional convective flows, several cases of supercritical Rayleigh numbers were simulated using different initial conditions cor-

Table 1. Results of grid-size tests for $\theta_m = 0.5$

Ra_L	Mesh	$\bar{\psi}_{max}$	$\Delta\bar{\psi}_{max}/\bar{\psi}_{max}$	$\bar{\psi}_{min}$	$\lvert\Delta\bar{\psi}_{min}\rvert/\lvert\bar{\psi}_{min}\rvert$	f
6×10^4	21×121	16.455	0.1075	−35.597	0.1218	36.39
	31×161	16.411	0.1083	−35.568	0.1140	35.71
	41×201	16.401	0.1078	−35.545	0.1100	35.26
10^5	31×161	36.458	0.1227	−60.939	0.1771	48.96
	41×201	35.764	0.1222	−60.019	0.1767	48.22
	51×241	35.435	0.1219	−59.653	0.1772	47.91

responding to results at both lower and higher Rayleigh numbers. For instance, for $Ra_L = 6\times10^4$ at $\theta_m = 0.5$ the simulations using as initial conditions the flow fields corresponding to $Ra_L = 5\times10^4$ and 10^5 yielded the same time-asymptotic evolution of the convective flow and the same oscillatory frequencies.

For a stable and accurate explicit double-precision calculation, a time step of the order of 10^{-6} was found to be sufficiently small, insuring that at least 5000 time increments were used to resolve the fine temporal scale of oscillatory convection flow for one period. Grid resolution independence was assured by comparing solutions obtained on various grid systems, as exemplified in Table 1 for two different Rayleigh numbers at $\theta_m = 0.5$. In the table some flow characteristics of the oscillatory convection obtained at two Rayleigh numbers, such as the dimensionless oscillation frequency f, the periodically mean values of the stream function extrema, $\bar{\psi}_{max}$ and $\bar{\psi}_{min}$, and their fractions of fluctuation, $\Delta\bar{\psi}_{max}/\bar{\psi}_{max}$ and $\Delta\bar{\psi}_{min}/|\bar{\psi}_{min}|$, are presented. From the table it is evident that 31×161 mesh at $Ra_L = 6\times10^4$ can yield an accuracy of better than 1.3, 0.01 and 0.01%, respectively, for f, $\bar{\psi}_{max}$, and $\bar{\psi}_{min}$. Accordingly, in the present study a grid system of 31×161 was used for the simulations of the Rayleigh numbers up to 10^5, while a finer mesh of 41×201 was employed for those of beyond 10^5.

Furthermore, the accuracy of the present numerical code is established through a series of validation simulations. Table 2 compares results of the simulations for steady state natural convection in a cold water-filled annulus of unit aspect ratio with the corresponding results presented in [6]. The predicted results of $\overline{Nu}_{i,m}$ and ψ_{max} from the present simulations apparently agree well with those of [6]. Further validation simulations were conducted for the problem of natural convection of air in vertical tall annuli of radius ratio 1.125 [14] and a good agreement of the averaged heat transfer results has been found.

Table 2. Comparison of the results for steady state natural convection of cold water in a vertical annulus of $A = 1$, $RR = 2$, and $\theta_m = 0.5$

	$(\overline{Nu}_{i,m}, \psi_{max})$	
Ra_L	Lin and Nansteel [6]	Present simulation
10^4	(1.738, 0.281)	(1.758, 0.284)
10^5	(3.521, 0.998)	(3.534, 1.006)
10^6	(7.136, 2.043)	(7.145, 2.102)

RESULTS AND DISCUSSION

Numerical simulations for the transient natural convection of cold water in the vertical annulus of aspect ratio 8 and radius ratio 2 have been undertaken with varying Rayleigh number for two values of the density inversion parameter $\theta_m = 0.4$ and 0.5, where the density inversion phenomenon may affect the convective flow significantly. The prominent effect of increasing the Rayleigh number under a fixed θ_m of 0.4 or 0.5 on the evolution of flow structure and temperature distribution will be illustrated by contour plots of streamlines and isotherms. The solid and dashed lines in the contour plots represent, respectively, the positive and negative values of the physical quantity of interest. Also superimposed on the contour maps is the maximum density contour denoted by the heavy dashed line.

Results of $\theta_m = 0.4$

The simulations for $\theta_m = 0.4$ were started with $Ra_L = 5\times10^4$ using a quiescent water at a uniform temperature of $\theta = 0$ as the initial conditions. Development of the natural convection of water within the annulus was initiated by suddenly raising temperature of the inner vertical wall to a constant value of $\theta = 1$. For $Ra_L = 5\times10^4$ the simulation was found to approach steady state through a transient development of flow structure and temperature field as illustrated in Fig. 2. As can be noticed in the sequence of streamline plots of Fig. 2, during the early stage, the counterclockwise circulation flow (outer circulation) dominates the annulus with the maximum density contour located adjacent and parallel to the inner wall. At $\tau = 0.05$ a weak clockwise eddy confined roughly by the maximum density contour can be seen to arise at the bottom left corner of the annulus. As the isothermal heating further continues at the inner wall, the clockwise eddy (inner circulation) strengthens increasingly and grows in size with its vortex center moving upward; while the outer circulation becomes suppressed accordingly. At $\tau \geqslant 0.1$, as shown in Fig. 2, vortex splitting phenomenon is detected within both the inner and outer circulation regions,

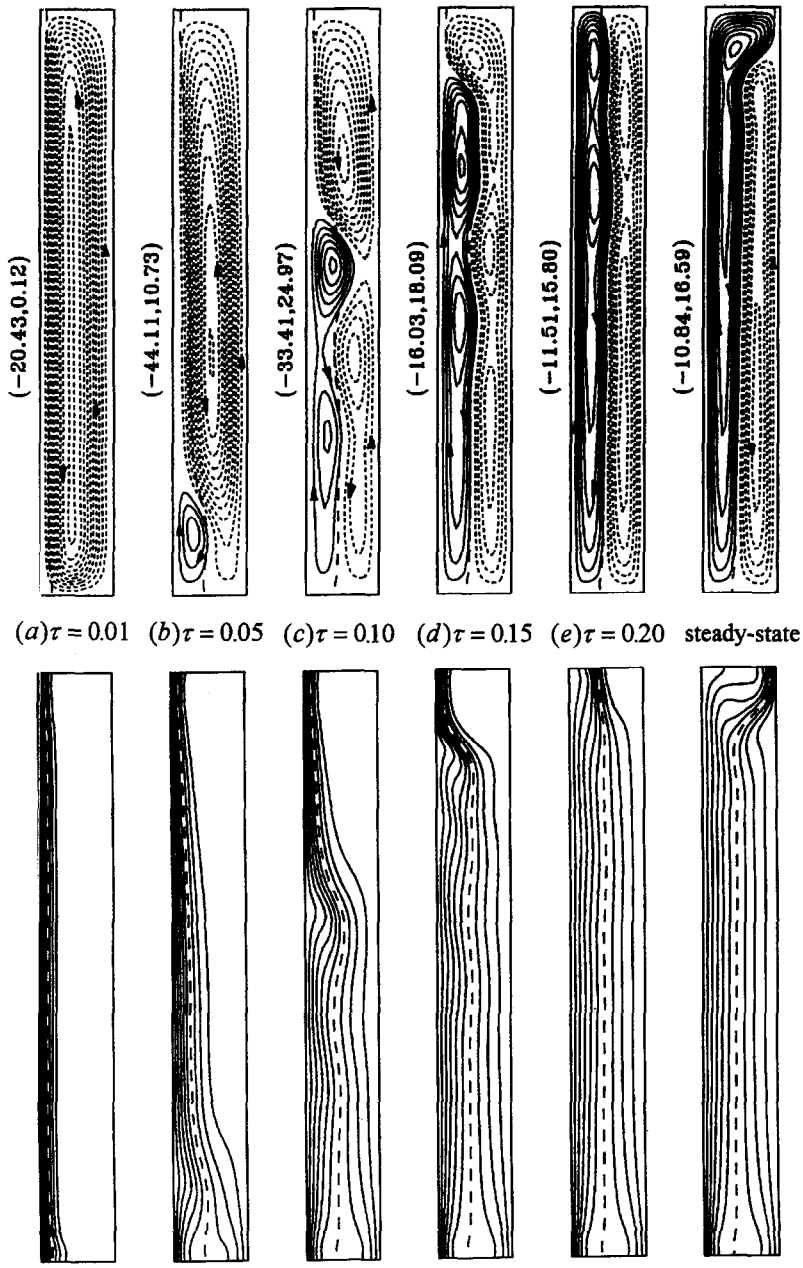

Fig. 2. Evolution of flow structure (upper) and temperature distribution (lower) in the annulus of $A = 8$ and $RR = 2$ at $Ra_L = 5 \times 10^4$ with $\theta_m = 0.4$.

within which an upward-drifting multicellular flow structure is accordingly formed. In accordance with the unsteady multicellular flow development in the annulus, the maximum density contour exhibits an upward traveling wave movement on its transverse penetration process away from the inner wall. As the upward-drifting secondary clockwise eddy reaches the ceiling of the annulus, the vortex-splitting process goes into reverse, giving way to the occurrence of eddy-merging within the inner and outer circulation regions. As the steady state is reached, the global flow field in the annulus features a contra-rotating bicellular structure demarcated roughly by the maximum density contour, as depicted in Fig. 2. The downward flow stream along the maximum density contour can be viewed as a sinking maximum density jet from the top corner of the outer wall. Moreover, a co-rotating bicellular structure can be detected to persist within the inner circulation with the dominant eddy residing in the top region of annulus. As a result, a "neck-down" region is formed of the inner circulation. Accordingly, as illustrated by the steady state

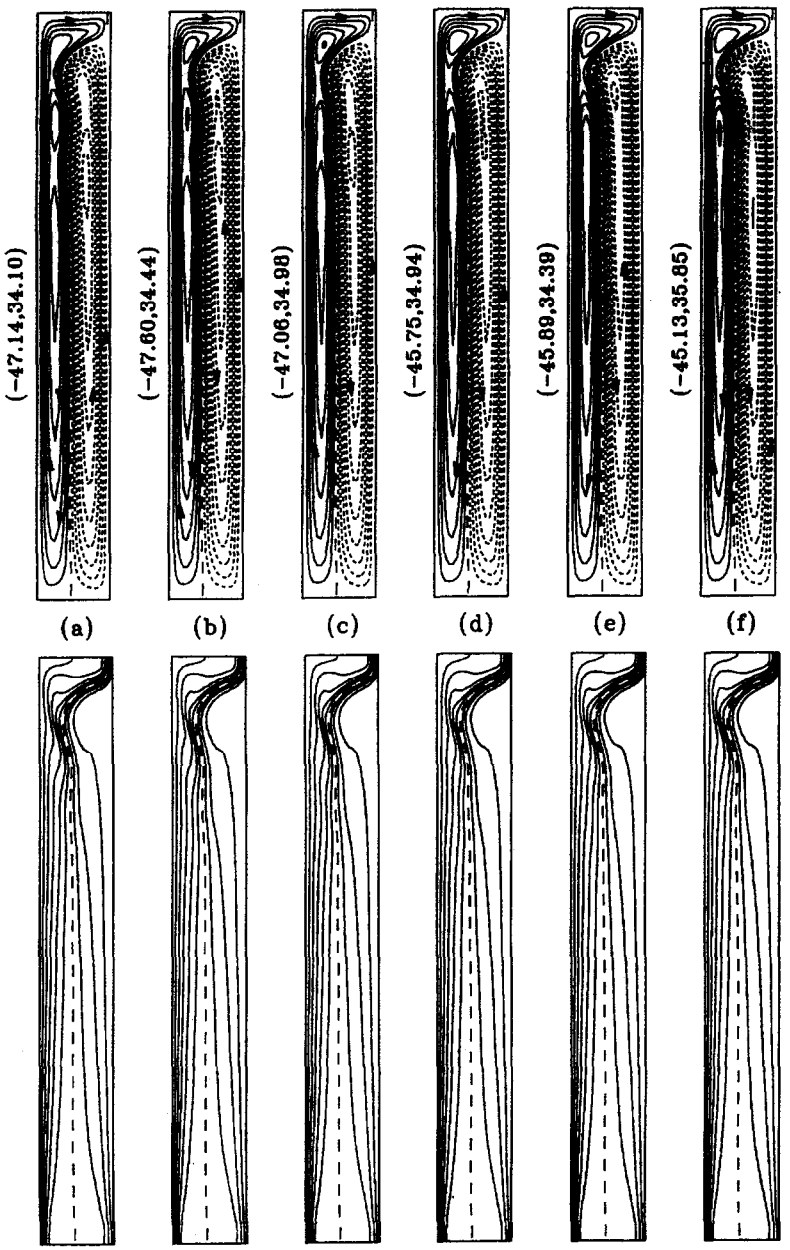

Fig. 3. Cyclic variation of streamlines (upper) with $\Delta\psi = 5$ and isotherms (lower) with $\Delta\theta = 0.1$ for $Ra_L = 2 \times 10^5$ and $\theta_m = 0.4$.

isotherms in Fig. 2, the top portion of the maximum density contour becomes deformed, slanting toward the outer wall. For the subsequent simulations for the Rayleigh number beyond 5×10^4 up to 10^5, which are based on the solution obtained for the previously lower Rayleigh number as the initial condition, the steady state nature convection persists with the increasingly intensified convective flow in the annulus. At $Ra_L = 10^5$ the steady state buoyant flow in the annulus (not shown here) features a contra-rotating bicellular structure of approximately equal strength.

A further increase of the Rayleigh number to 2×10^5 yielded a temporally oscillatory convective flow with a dimensionless frequency of $f = 94.7$. Figure 3 displays the cyclic variation of the streamlines and isotherms of the fully developed simple periodic convection prediction at $Ra_L = 2 \times 10^5$. An overview of the streamline plots in Fig. 3 reveals that a cyclic sequence of splitting and then merging of the upward-drifting secondary vortices takes place within both the inner and outer circulation in the annulus. Accordingly, a cyclic wavy movement the maximum density contour can be discerned around the neck-down region. From the corresponding sequence of isotherms in Fig. 3 it is

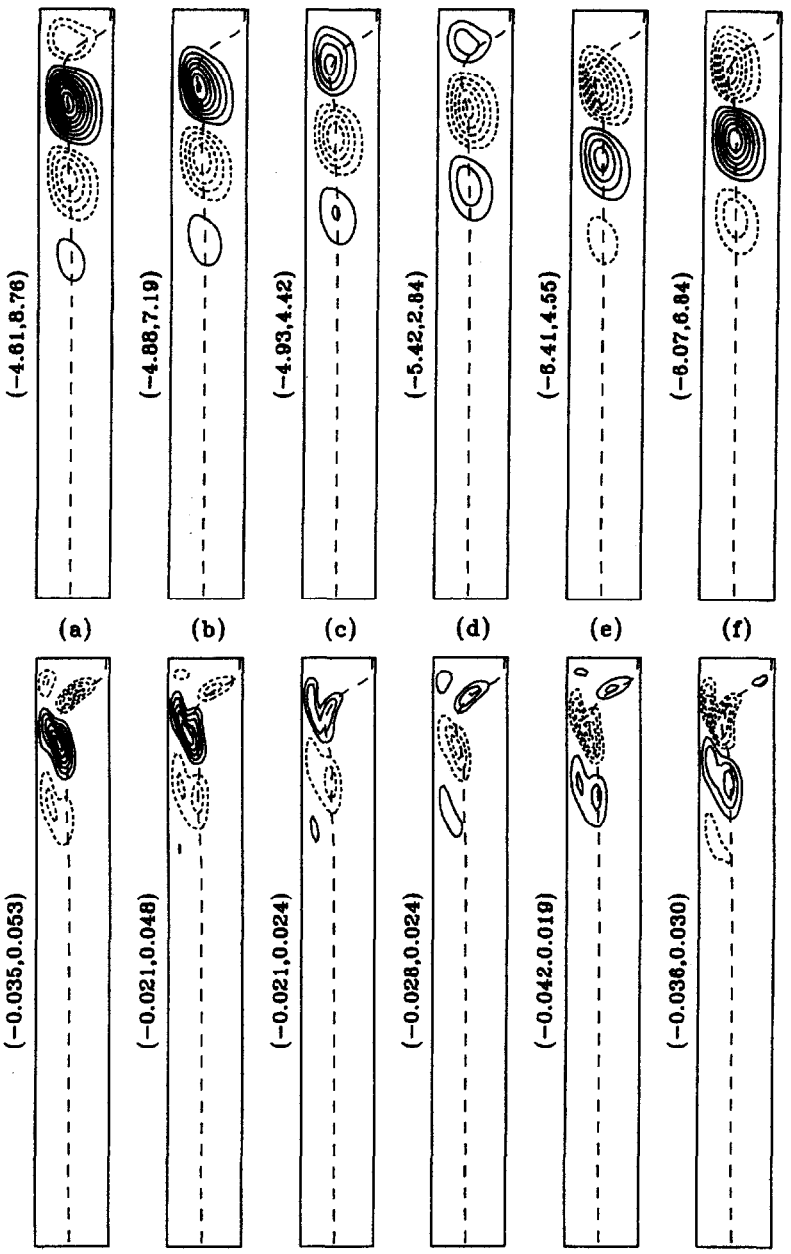

Fig. 4. Cyclic sequence of the fluctuating stream function (upper) and temperature (lower) fields for $Ra_L = 2 \times 10^5$ and $\theta_m = 0.4$ at the time instants corresponding to those in Fig. 4. The contour increments are $\Delta\psi' = 1$ and $\Delta\theta' = 0.008$. Negative fluctuating isovalues are denoted by dotted lines.

clear that the thermal boundary layer along the inner wall features a cyclic variation of the wavy isotherms around the neck-down region in accordance with the upward-drifting-through of the clockwise secondary vortex. Further physical insight of the oscillatory convection can be furnished by plotting the corresponding spatial distributions of the fluctuating magnitude of stream function and temperature, which were evaluated by subtracting the local time-averaged value from the local instantaneous value of the stream function or temperature in every grid point of the annulus. Figure 4 shows the instantaneous distributions of the fluctuating magnitude of the stream function and temperature at the instants corresponding to those shown in Fig. 3. The positive and negative fluctuating magnitudes of stream function and temperature are denoted by the solid and dashed contours, respectively. An overview of Fig. 4 reveals that the fluctuations in the flow and temperature fields are confined to the upper half portion of the annulus and display a periodic sequence of initiation, growth and then fadeout while upward-drifting, and finally extinction at the

ceiling of the annulus. Specifically, the cyclic evolution of stream function fluctuation appears to initiate around the mid-height of the annulus and then grow as it drifts upward along the maximum density contour. The upward-drifting fluctuation structure of stream function reaches a peak magnitude around the neck-down region and then gives way to decay as it moves further upward, but not along the maximum density contour any more. On the other hand, a relatively complicated cyclic variation can be observed of the corresponding sequence of temperature fluctuation distributions in Fig. 4. Most distinctly, the temperature fluctuations are mostly confined to the inner circulation region. After its inception, the upward-drifting temperature fluctuation structure appears to penetrate across the maximum density contour, wherein experiencing a downward drag by the sinking maximum density jet flow. As a result, a center-splitting of the temperature fluctuation structure arises featuring a twin-peak structure with one of the fluctuation peaks centered on the maximum density contour. The twin-peak temperature fluctuation attains its maximum magnitude around the neck-down region, where the waviness of the isotherms along the inner wall and of the maximum density contour is most visible. Afterwards, the twin-peak structure of temperature fluctuation can be seen to separate gradually into two isolated structures as it drifts through the neck-down region. One of the separated fluctuation structures then moves along the rightward-slanting maximum density contour and finally dies out at the outer wall; while the other separated structure continues its upward drifting along the inner wall reaching the ceiling of the annulus.

Simulations for $\theta_m = 0.4$ were further carried out by progressively increasing the Rayleigh number up to 9×10^5. The solutions to these cases all evolve to a simple periodic convection with an increasingly higher frequency, which can be well correlated with the Rayleigh number and Prandtl number as follows:

$$f/(Ra_L^2\, Pr)^{1/3} = 0.0114, \quad 1.4 \times 10^5 \leqslant Ra_L \leqslant 9 \times 10^5 \tag{8}$$

with an averaged and maximum deviation of 1.2 and 1.8%, respectively. It can be inferred from eqn (8) that the dimensional oscillation frequencies f^+ at the supercritical Rayleigh numbers can be scaled well with $(rsp \cdot g\,\Delta T^b)^{2/3} v^{-1/3}$, which is the characteristic frequency of vertical natural convection boundary layer flow [15].

Results of $\theta_m = 0.5$

Under the condition of $\theta_m = 0.5$, progressively increase of Ra_L up to 5×10^4 the steady state natural convection has been obtained for the time-dependent simulations. The steady state buoyancy-driven flow in the annulus characterizes, in general, with a globally bicellular structure. Somewhat opposite to that found at $\theta_m = 0.4$, the outer circulation is the dominant flow structure in the annulus with the maximum density contour slanting toward the inner wall, as exemplified by the steady state flow pattern and temperature distribution at $Ra_L = 5 \times 10^4$ shown in Fig. 5. A neck-down region of the outer circulation is clearly formed in the upper portion of the annulus.

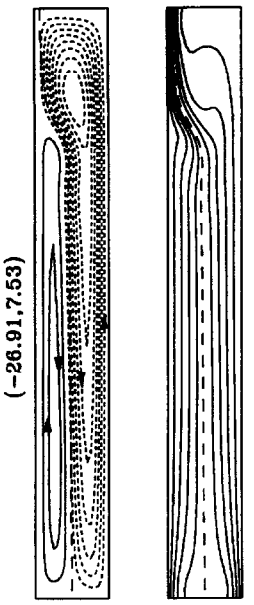

Fig. 5. Steady state results of streamline pattern (left) and isotherm distribution (right) for $Ra_L = 5 \times 10^4$ and $\theta_m = 0.5$.

At $Ra_L = 6 \times 10^4$ the oscillatory convection in the annulus was first detected with a frequency of $f = 35.71$. The cyclic variation of the oscillatory convective flow and temperature fields at $Ra_L = 6 \times 10^4$ was illustrated in Fig. 6. Similar to that detected in Fig. 3 for $Ra_L = 2 \times 10^5$ at $\theta_m = 0.4$, the periodic flow structure shown in Fig. 6 features a cyclic sequence of onset, upward drifting, growing, and fadeout of the split vortices within both the inner and outer circulation, which is synchronized with the upward traveling wave motion of the maximum density contour. Also, as revealed in the corresponding sequence of temperature distribution shown in Fig. 6, the thermal boundary layers along both the inner and outer walls, in synchronization with the periodic wave motion of the maximum density contour, display a sequence of upward traveling wave trains. Furthermore, from the corresponding cyclic spatial structures of the fluctuating stream function and temperature presented in Fig. 7, one can observe that both the fluctuating quantities undergo a similar cyclic variation: onset at the bottom quarter region, whereupon the maximum density contour starts it meandering; then growing in size and magnitude as they drift upward along the mid-vertical line of the annulus; finally fading out at the ceiling of the annulus. A closer examination of the fluctuation structures reveals that the consecutive

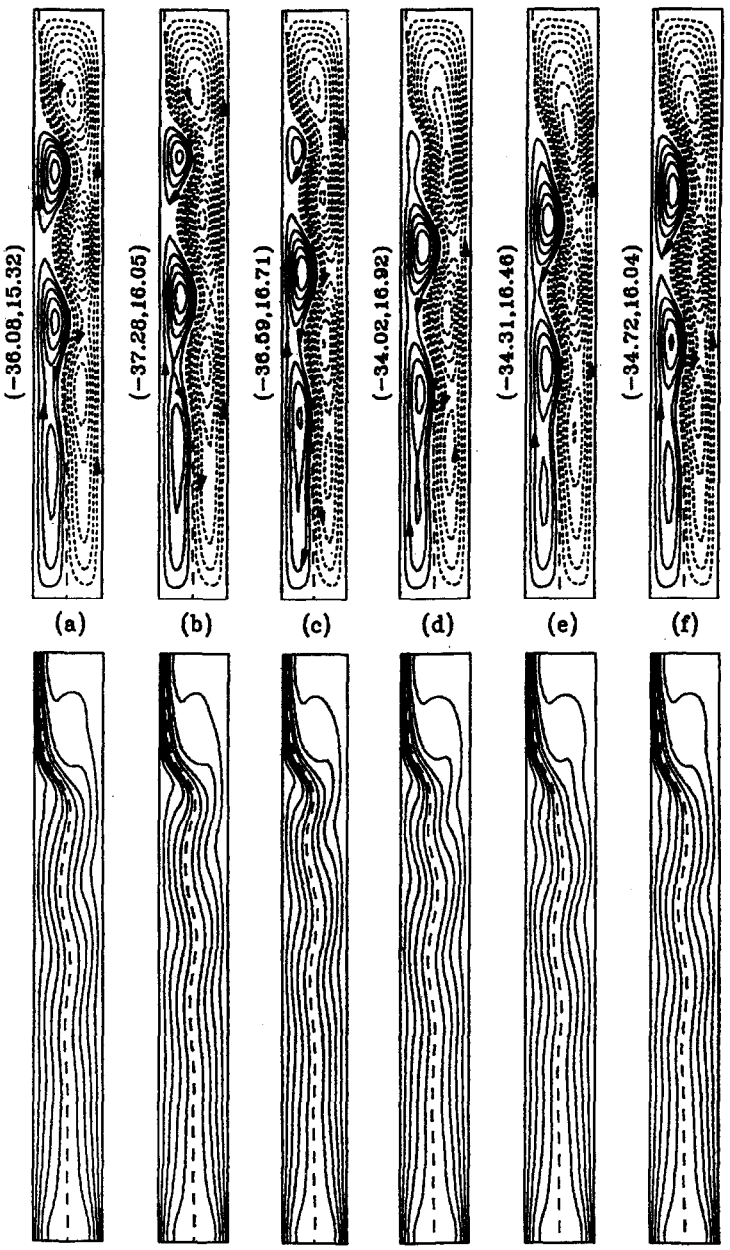

Fig. 6. Cyclic variation of streamlines (upper) and isotherms (lower) for $Ra_L = 6 \times 10^4$ and $\theta_m = 0.5$.

fluctuation structures of alternate sign concentrate in the core region of the annulus and have their peaks always centered to the left or the right sides of the somewhat wavy maximum density contour. Similar to that found at $\theta_m = 0.4$ (Fig. 4), the temperature fluctuation structure shown in Fig. 7 undergoes a process of center-splitting and then separating into two isolated structures as it drifts toward the neck-down region along the maximum density contour. One of the separated temperature fluctuation structures further moves along the leftward-slanted maximum density contour; while the other structure appears to be advected by the outer circulation toward the outer wall.

At higher Rayleigh numbers $Ra_L = 7 \times 10^4 \sim 10^5$, the self-sustained oscillatory convection persists in the annulus with increasingly higher level of unsteadiness and complexity, as exemplified by the periodic variation of the flow structure and temperature distribution at $Ra_L = 10^5$ shown in Fig. 8. Evidently, the wavy motion of the maximum density contour as well as of the isotherms is greatly amplified. Accordingly, as shown in Fig. 9, the local Nusselt number profiles at the inner and outer walls at the time instants cor-

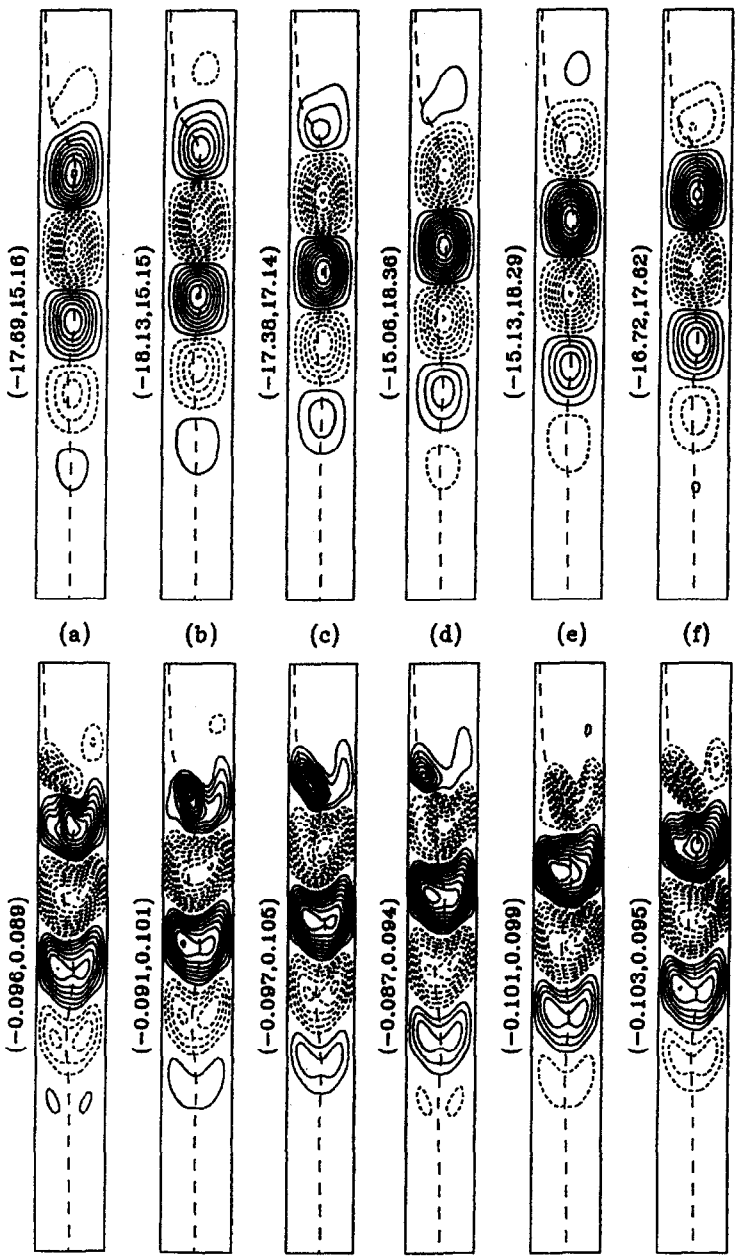

Fig. 7. Cyclic sequence of the fluctuating stream function (upper) and temperature (lower) fields for $Ra_L = 6 \times 10^4$ and $\theta_m = 0.5$.

responding to those of Fig. 8 display a traveling wavy distribution. Moreover, the oscillation frequencies at the supercritical Rayleigh numbers, as that found at $\theta_m = 0.4$, can be well correlated with the Rayleigh number as

$$f/(Ra_L^2\, Pr)^{1/3} = 0.00995, \quad 5.2 \times 10^4 \leqslant Ra_L \leqslant 10^5 \qquad (9)$$

with an averaged and maximum deviation of 0.76 and 3.2%, respectively.

Critical Rayleigh numbers

The critical Rayleigh number for the laminar transition through Hopf bifurcation into periodic oscillatory convection in the cold-water annulus was determined by computing several supercritical simulations and extrapolating the squared amplitudes of the fluctuations to zero. The critical Rayleigh numbers $Ra_{L,cr}$ for $\theta_m = 0.4$ and 0.5 are found to be $1.40 \times 10^5 \pm 3300$ ($Ra_{H,cr} = 7.168 \times 10^7$) and $5.200 \times 10^4 \pm 60$ ($Ra_{H,cr} = 2.662 \times 10^7$), respectively. The critical Rayleigh number at $\theta_m = 0.4$ is more than two times of that at $\theta_m = 0.5$. This clearly reflects that the transition into oscillatory convection in the annulus has a strong bearing with the density inversion phenomenon of cold water.

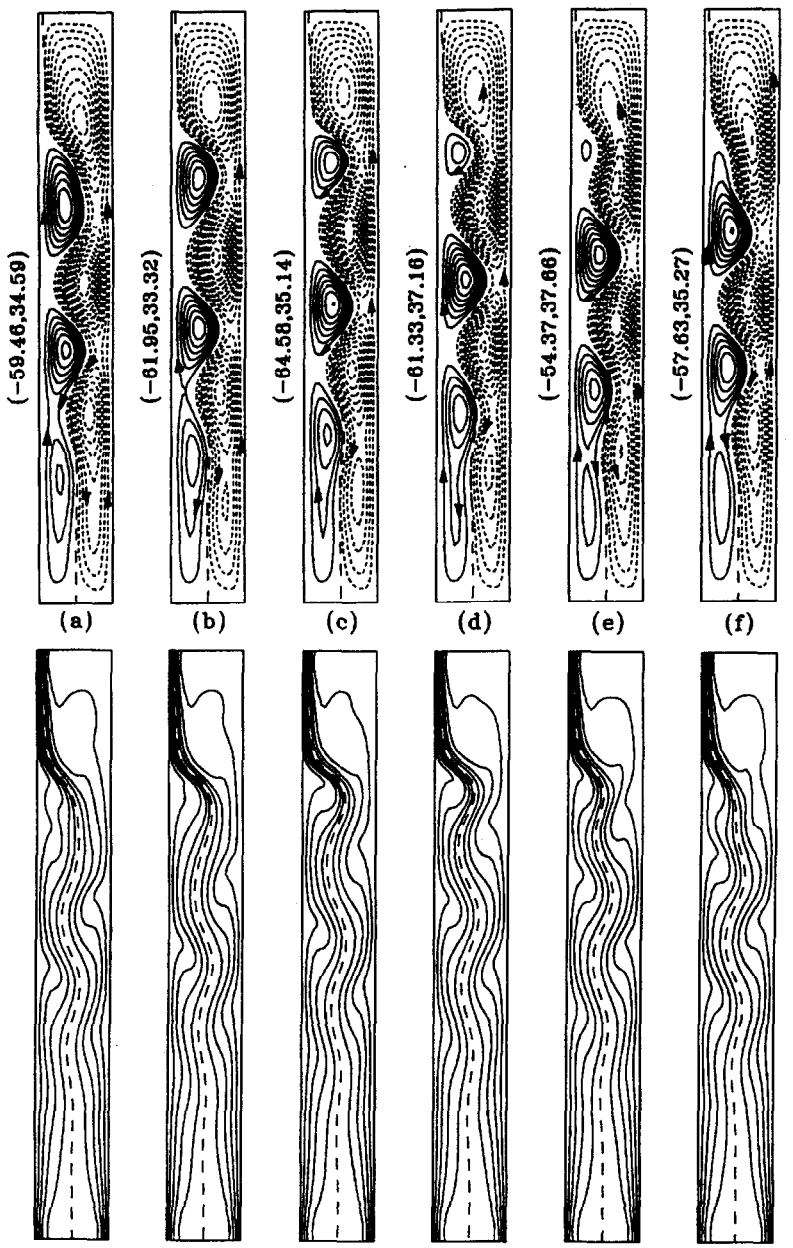

Fig. 8. Cyclic sequence of the fluctuating stream function (upper) and temperature (lower) fields for $Ra_L = 10^5$ and $\theta_m = 0.5$.

Nature of instability mechanism

Further insight into nature of the instability mechanism of natural convection in the cold water-filled annulus can be obtained by examining the production terms of the fluctuating kinetic energy in the term group III of eqn (7), which can be due to the flow shear and/or the buoyancy force. To this end, spatial distributions of the production of fluctuating kinetic energy due to flow shear and due to buoyancy are obtained by integrating eqn (7) over one period of the oscillation.

Figure 10 illustrates the resulting distributions for the oscillatory convection at $\theta_m = 0.4$ shown in Fig. 3. At $Ra_L = 2 \times 10^5$ and $\theta_m = 0.4$, the shear-generated fluctuating kinetic energy, as shown in Fig. 10(a), mainly exists on either side of the maximum density contour, particularly in the neck-down region. This shear-induced instability, however, is not as dominant as the positive production region due to buoyancy displayed in Fig. 10(b). The positive buoyancy-induced production is present mostly in the upper quarter region of the vertical boundary layer along the inner wall. Meanwhile, in the counter-clockwise outer circulation region relatively small contribution

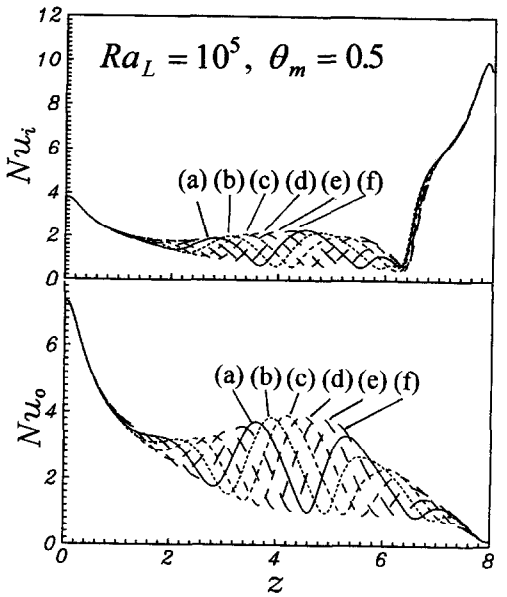

Fig. 9. Cyclic variation of the local Nusselt number profiles at the inner and outer walls of the annulus at the time instants corresponding to those in Fig. 8.

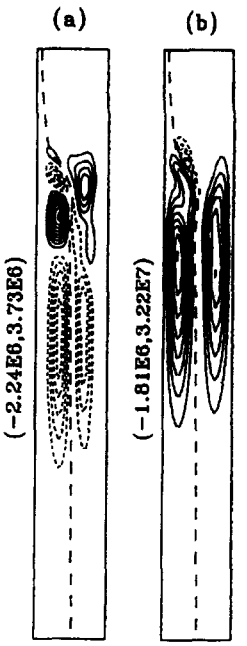

Fig. 11. Distribution of local production of fluctuating kinetic energy due to (a) flow shear and (b) buoyancy for $Ra_L = 6 \times 10^4$ and $\theta_m = 0.5$.

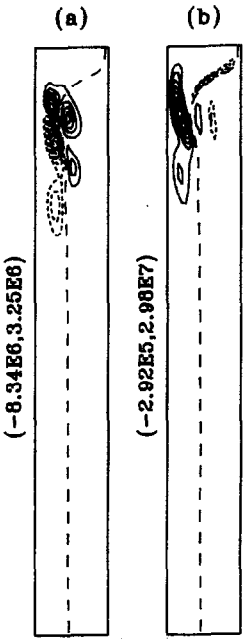

Fig. 10. Distribution of local production of fluctuating kinetic energy due to (a) flow shear and (b) buoyancy for $Ra_L = 2 \times 10^5$ and $\theta_m = 0.4$. Negative isovalues are denoted by dotted lines.

to the buoyancy-induced production can be detected along the wavy maximum-density contour around the neck-down region. It can then be concluded from Fig. 10 that buoyancy is the primary source for production of the fluctuating kinetic energy. This can be further confirmed by checking the total fluctuating kinetic energy production budget, which was obtained by integrating the local production of fluctuating kinetic energy shown in Fig. 10 over the entire annulus. The result reveals that for the present case the production of total fluctuating kinetic energy is contributed completely by the buoyancy; while the flow shear contributes negatively (−9.1%) to the production of total fluctuating kinetic energy. This indicates that the transition into oscillatory convection of cold water in the annulus for $\theta_m = 0.4$ is a buoyancy-driven or thermal instability.

Moreover, calculations of the fluctuating kinetic energy production for the supercritical Rayleigh numbers above 2×10^5 up to 9×10^5 under $\theta_m = 0.4$ show that the total production of the fluctuating kinetic energy for each case is completely contributed by the buoyancy, further indication of a buoyancy-driven instability.

Similar conclusion of buoyancy-driven instability can be drawn for the oscillatory convection in the annulus under $\theta_m = 0.5$. As demonstrated in Fig. 11 for $Ra_L = 6 \times 10^4$ and $\theta_m = 0.5$, the local production of fluctuating kinetic energy due to buoyancy exhibits a somewhat symmetric distribution with respect to the time-averaged maximum density contour. The buoyancy is the dominant source for fluctuating kinetic energy production. Moreover, similar to that found for $\theta_m = 0.4$, the total production of the fluctuating kinetic energy production in the annulus is found to be solely contributed by the buoyancy.

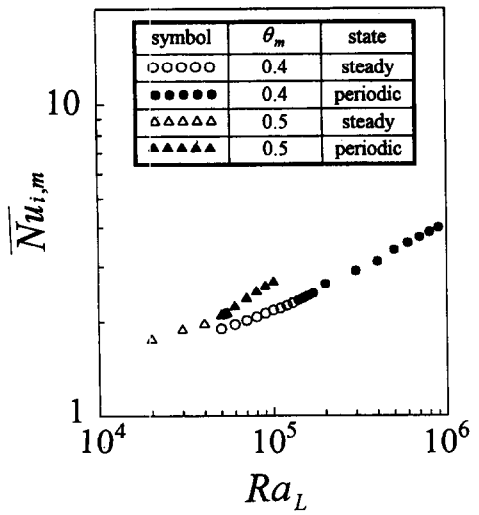

Fig. 12. Variation of the steady state or periodically mean, surface-averaged Nusselt number with the Rayleigh number.

Heat transfer correlation

Finally, the steady-state or the periodically mean results of the surface-averaged heat transfer rate across the vertical annulus are presented by means of an averaged Nusselt number at the inner wall of the annulus, $\overline{Nu}_{i,m}$ which is defined as

$$\overline{Nu}_{i,m} = \begin{cases} \dfrac{1}{A}\displaystyle\int_0^A Nu_i \, dz \quad \text{(steady state)} \\ \dfrac{1}{p}\displaystyle\int_0^p \left[\frac{1}{A}\int_0^A Nu_i \, dz\right] d\tau \\ \qquad \text{(periodic oscillatory state)} \end{cases} \quad (10)$$

Here p is the dimensionless period of the oscillatory convection. The data of $\overline{Nu}_{i,m}$ were plotted against the Rayleigh number as shown in Fig. 12. For the ranges of Rayleigh number considered, the averaged heat transfer rate at a given Rayleigh number of $\theta_m = 0.5$ appears to be always markedly higher than that for $\theta_m = 0.4$, indicative of the influence of density inversion on heat transfer across the annulus. By means of the least squares regression, a correlation for $\overline{Nu}_{i,m}$ vs the Rayleigh number can be obtained as:

$$\overline{Nu}_{i,m} = 0.101 Ra_L^{0.266} \quad (11a)$$

with an averaged and maximum deviation of 1.7 and 3.1%, respectively, for $5 \times 10^4 \leqslant Ra_L \leqslant 9 \times 10^5$ at $\theta_m = 0.4$; and

$$\overline{Nu}_{i,m} = 0.115 Ra_L^{0.272} \quad (11b)$$

with an averaged and maximum deviation of 2.7 and 3.7%, respectively, for $2 \times 10^4 \leqslant Ra_L \leqslant 10^5$ at $\theta_m = 0.5$.

CONCLUDING REMARKS

Direct numerical simulations of time-dependent axisymmetric buoyancy-driven flow of cold water in a vertical cylindrical annulus of aspect ratio 8 and radius ratio 2 clearly reveal that the laminar transition to self-sustained oscillatory convection has a strong bearing with the density inversion phenomenon of cold water. The critical Rayleigh number for $\theta_m = 0.4$ is found to be more than two times of that corresponding to $\theta_m = 0.5$. For both values of θ_m, the transition from steady state to unsteady convection features the characteristics of a supercritical Hopf bifurcation. Moreover, the transition into unsteadiness mechanism has been manifested to be buoyancy-driven instability. The oscillatory convection in the annulus is characterized by the appearance of unsteady multicellular structure within the globally contra-rotating bicellular flow regions of cold water. The oscillation frequencies detected at the supercritical Rayleigh numbers in both values of θ_m can be scaled well with $(rsp \cdot g \Delta T^b)^{2/3} \nu^{-1/3}$. Further simulations for a wider range of θ_m as well as on the geometric effects of radius ratio and aspect ratio of the annulus are certainly needed in the future study.

Acknowledgements—This research was supported by the National Science Council of Republic of China on Taiwan through Project Nos. NSC83-2212-E006-110 and NSC84-2212-E006-013. The necessary computing facility and time are kindly provided by the National Center for High-Performance Computing of NSC. The constructive comments of the reviewers are sincerely appreciated.

REFERENCES

1. Inaba, H. and Fukuda, T., Natural convection in an inclined square cavity in regions of density inversion of water. *J. Fluid Mech.*, 1984, **142**, 363–381.
2. Lin, D. S. and Nansteel, N. W., Natural convection heat transfer in a square enclosure containing water near its density maximum. *Int. J. Heat Mass Transfer*, 1987, **30**, 2319–2329.
3. Tong, W. and Koster, J., Density inversion effect on transient natural convection in a rectangular enclosure. *Int. J. Heat Mass Transfer*, 1994, **37**, 927–938.
4. Vasseur, P., Robbilard, L. and Chandra Shekar, B., Natural convection heat transfer of water within a horizontal cylindrical annulus with density inversion effects. *J. Heat Transfer*, 1983, **105**, 117–123.
5. Ho, C. J. and Lin, Y. H., Natural convection heat transfer of cold water within an eccentric horizontal cylindrical annulus. *J. Heat Transfer*, 1988, **110**, 894–900.
6. Lin, D. S. and Nansteel, M. W., Natural convection in a vertical annulus containing water near the density maximum. *J. Heat Transfer*, 1987, **109**, 899–905.
7. Ho, C. J. and Lin, Y. H., Natural convection of cold water in a vertical annulus with constant heat flux on the inner wall. *J. Heat Transfer*, 1990, **112**, 117–123.
8. McFadden, G. B., Coriell, S. R., Boisvert, R. F. and Glicksman, M. E., Asymmetric instabilities in buoyancy-driven flow in a tall vertical annulus. *Phys. Fluids*, 1984, **27**, 1359–1361.
9. Gebhart, B. and Mollendorf, J. C., A new density relation for pure and saline water. *Deep Sea Res.*, 1977, **24**, 831–848.
10. Janssen, R. J. A. and Henkes, R. A. W. M., Influences of Prandtl number on instability mechanisms and tran-

sition in a differentially heated square cavity. *J. Fluid Mech.*, 1995, **290,** 319–344.
11. Simons, T. J., Circulation modes of lakes and inland seas. *Can. Bul. Fish. Aquatic Sci.*, 1980, **203,** 1–146.
12. Leonard, B. P., A convectively stable, third-order accurate finite difference method for steady two-dimensional flow and heat transfer. *Numerical Properties and Methodologies in Heat Transfer* (ed. T. M. Shih), pp. 211–226, Hemisphere, Washington, D.C., 1983.
13. Peyret, R. and Taylor, T. D., *Computational Methods for Fluid Flow*. Springer-Verlag, New York, 1983.
14. Lee, Y. and Korpela, S. A., Structure of multi-cellular natural convection in a tall annulus. *Heat Transfer*—1982, Vol. 2, pp. 221–226, 1982.
15. Gebhart, B. and Mahajan, R., Characteristic disturbance frequency in vertical natural convection flow. *Int. J. Heat Mass Transfer*, 1975, **18,** 1143–1148.